IEEE Access
Multidisciplinary | Rapid Review | Open Access Journal

Received November 19, 2018, accepted December 3, 2018, date of publication December 17, 2018,
date of current version January 11, 2019.

Digital Object Identifier 10.1109/ACCESS.2018.2886796

On the Modeling of Near-Field Scattering of Vehicles in Vehicle-to-X Wireless Channels Based on Scattering Centers

GUANGKAI LI[1,2], (Student Member, IEEE), BO AI[1,2], (Senior Member, IEEE), GORDON L. STÜBER[3], (Fellow, IEEE), KE GUAN[1,2], (Member, IEEE), AND GUOWEI SHI[4]

[1]State Key Laboratory of Rail Traffic Control and Safety, Beijing Jiaotong University, Beijing 100044, China
[2]Beijing Engineering Research Center of High-Speed Railway Broadband Mobile Communications, Beijing Jiaotong University, Beijing 100044, China
[3]School of Electrical and Computer Engineering, Georgia Institute of Technology, Atlanta, GA 30332, USA
[4]China Academy of Telecommunication Research, Beijing 100191, China

Corresponding author: Bo Ai (boai@bjtu.edu.cn)

This work was supported in part by the National Key Research and Development Program under Grant 2016YFE0200900 and Grant 2016YFB1200102-04, in part by the NSFC under Grant 61725101 and Grant 61771036, in part by the Beijing Natural Haidian Joint Fund under Grant L172020, in part by Beijing Natural Fund under Grant L161009, in part by the Major Projects of Beijing Municipal Science and Technology Commission under Grant Z181100003218010, in part by the State Key Lab of Rail Traffic Control and Safety under Grant RCS2017ZZ005, in part by the Fundamental Research funds for the central universities under Grant 2017RC03, and in part by the Teaching Reform Project under Grant 134496522.

ABSTRACT Efficient and reliable vehicle-to-X (V2X) wireless communication requires a deep understanding of the associated propagation channels. However, V2X channels are complicated due to the complex traffic phenomena, and thus extensive propagation studies are required to characterize these channels. This paper considers the effects of vehicle scattering on V2X channels. Most existing techniques that address vehicle scattering are imperfect, due to deficiencies in their computational accuracy and efficiency. In this paper, the tradeoff between computational accuracy and efficiency is addressed by proposing an analytical model based on the concept of scattering centers (SCs). The model can efficiently predict near-field bi-static scattering of vehicles with good accuracy. Also, to make the model widely acceptable, a general methodology of extracting SCs is carefully derived. Then, three standard vehicles (car, van, and truck) are employed for evaluating the performance of the model. The results indicate that the model is useful for reconstructing vehicle scattering in V2X channels.

INDEX TERMS Propagation channels, scattering centers (SCs), vehicle scattering, vehicle-to-X (V2X) communications.

I. INTRODUCTION

Vehicle-to-X (V2X) wireless communication has received much attention in recent years due to its potential of providing road safety (e.g., collision detection), green transportation (e.g., driver assistance, fleet management to reduce traffic congestion) and in-vehicle entertainment [1], [2]. V2X wireless communications, including the technologies of Vehicular Ad Hoc Networks (VANETs) [1] and Cooperative Vehicular Systems (CVSs) [3], are the promising approach of the emergence of Intelligent Transportation Systems (ITSs) [4]. Furthermore, to advance V2X technologies, V2X has recently been combined with some potential fifth-generation (5G) technologies, e.g., the massive multi-input multi-output (MIMO) system which involves hundreds of antennas [5].

It is generally accepted that a deep understanding of the relevant propagation channels is necessary for the effective design/optimization of wireless communication systems [6]. However, comparing some traditional communication channels (e.g., macro-/micro-cell communications channels [7], [8] and railway communications channels [9], [10]), V2X channels are more complicated due to the uncertainty/high-mobility of moving vehicles as well as the low antenna heights [11]. Therefore, although numerous investigations regarding V2X channels have been conducted [12], [13], some significant characteristics of V2X channels are still unstudied or understudied.

One of the most challenging topics is the modeling of vehicle scattering in V2X channels, in which the vehicles are

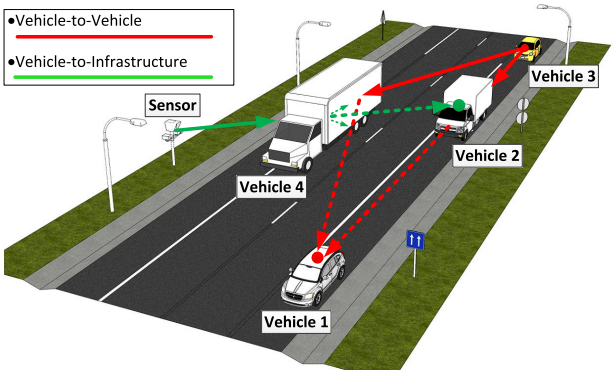

FIGURE 1. The transmitted signal from roadside sensor is blocked by vehicle 4; and the transmitted signal from vehicle 3 is blocked/ relayed by vehicle 2/vehicle 4.

either surrounding or are in between the transmitter (TX) and receiver (RX) [14], [15]. As illustrated by Fig. 1, the vehicles have the function of either blocking or relaying the transmitted signal. Both phenomena are impacted by vehicle scattering. For example, the channel measurement in [16] shows a blocking loss of over 20 dB by trucks. Moreover, Abbas *et al.* [17] and Meireles *et al.* [18] have analyzed and highlighted the importance of vehicles on V2X channels, and Matolak [11] has also stated that the effects of vehicles on V2X channels should be quantified.

The existing techniques for the inclusion of vehicle scattering in V2X channels can be classified as either stochastic models or deterministic models [15]. The former is based on the processing of measured channel data obtained from well-selected scenarios. The final outputs of the stochastic models are the statistics of some important V2X channel parameters (see [15], [19]–[23]). Although the stochastic models are widely accepted as reproducing V2X channels in a highly efficient way, the model itself is of limited functionality and unable to specifically quantify the effect of a given vehicle. The reason is the inherent deficiency of the stochastic model that requires enough channel samples to be lumped together in order to extract statistics. The analysis will be inevitably limited by the realistic channel conditions. For example, the measured channel data of [17] and [24] includes the scattering effects of cars, vans, and trucks. Thus, it will be impossible to single out a truck effect [15]. Moreover, Wang *et al.* [16] studied the blocking loss caused by a truck/van in a stochastic way, but the measurement scenario was quite simple in that the TX, truck/van, and RX were all in a line. Therefore, if the relative position of truck/van is different from the measurement scenario, the extracted stochastic model of [16] could not be expected to reproduce the required losses.

The deterministic models use numerical techniques for solving Maxwell's equations by taking into account the geometry of the environment. A higher precision of the geometry will undoubtedly increase the accuracy of the models, but it will also significantly increase computational complexity. In V2X channels, the common approaches of investigating vehicle scattering are based on an oversimplified geometry or rough solutions, which inevitably causes inaccuracy of the results [15]. For example, Rodriguez *et al.* [25] studied truck shadowing in V2X by using a ray-tracing (RT) technique [26] where the geometry of the truck was composed of only a few panels; Boban *et al.* [27] modeled the vehicle shadowing by using a simple knife-edge diffraction model; Vlastaras *et al.* [28] theoretically proposed a six-path model as a closed-form solution for a truck shadowing. Therefore, it is evident that there is an urgent need for modeling vehicle specific scattering effects on V2X channels, where the model has been given a balance between accuracy and computation time. It should noted that Buddendick and Eibert [29] have made great attempts to use the scattering centers (SCs) concept for solving this problem. The SCs concept is useful as it could model the complex vehicle scattering through a simple and sparse representation. However, the SCs studied in [29] were only learned from the Shooting and Bouncing Ray (SBR) technique which makes the model inflexible [30].

This paper derives an analytical model for directly predicting bi-static near-field scattering of vehicles in V2X channels, through an innovative extension of [30]. Since the proposed model is based on the well-known SCs concept, the efficiency and accuracy of the proposed model maintains good balance. Moreover, a general methodology of SCs extraction from the bi-static scattering field is also derived. Most notably, this is the first study to our knowledge to provide a general and complete solution for modeling vehicle scattering in V2X channels. Although the accuracy of the model varies slightly with different vehicles, the model is still a valuable technique. The main contribution of the paper can be considered as a two-step procedure. As detailed in Section III, in the first step, the complete far-field scattered field of vehicles is obtained by a full-wave analysis method (Physical Optics (PO) in this study), then, the SCs are extracted from the scattered field. The second step, as described in Section II, uses the extracted SCs to predict the near-field scattering of vehicles. Other than Sections II and III, the remainder of this paper is organized as follows. In Section IV, the accuracy of the models described in Sections II and III are validated, respectively, considering a car, a van, and a truck. Section V concludes the paper.

II. ANALYTICAL MODELING FOR BI-STATIC VEHICLE SCATTERING IN NEAR-FIELD

Scattering occurs when an electromagnetic (EM) wave hits an object (or scatterer) [31]. It is a common physical interaction that causes deviation of the wave propagation trajectory. Vehicles are considered as scatterers. According to different structures on the vehicle surface, the scattering can be classified into different scattering mechanisms. As can be seen in Fig. 2, the scattering mechanisms include specular reflection from planar surface (a), multiple scattering from a dihedral or trihedral corner (b), surface scattering from a curved surface (c) and edge/tip diffraction (d). Knowledge of the scattering mechanisms is the principal inspiration for some EM analysis solvers (e.g., Geometrical Optics (GO) and

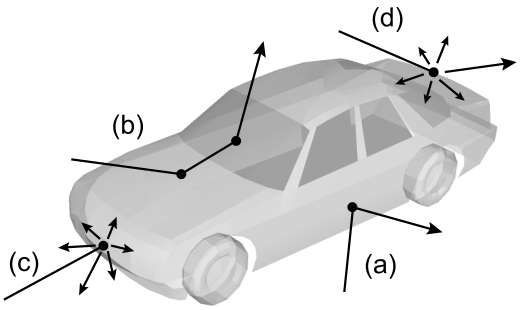

FIGURE 2. Different scattering mechanisms happening on a vehicle surface.

PO methods [32]). However, in V2X channel simulations, modeling the vehicle scattering directly by using the above scattering mechanisms would be highly inefficient [29].

In this study, the scattered power from vehicles is analytically modeled by radar methods, where the most important coefficient (known as the bi-static radar cross section (biRCS)) is calculated using SCs. The SCs can be considered as pre-abstracting/processing the above scattering mechanisms with virtual points. Furthermore, in V2X communication systems, the angle subtended between the TX, a vehicle and the RX is hardly equal to zero. Therefore, it is worth mentioning that all concepts discussed/adopted in this work are specifically corresponding to their bi-static cases, e.g., bi-static radar equation, biRCS, etc.

A. BI-STATIC RADAR EQUATION

In V2X channel simulations, the received scattered power from vehicles can be calculated by adopting the well-known radar equation [33]:

$$P_r = \frac{P_t G_t}{4\pi R_t^2} \times \frac{\sigma_{bi}}{4\pi R_r^2} \times \left(G_r A_{eff}\right) \tag{1}$$

where

- $P_{t/r}$ = transmitted/received-signal power (at antenna terminals),
- $G_{t/r}$ = TX/RX antenna gain,
- $R_{t/r}$ = distance between TX/RX and the centroid of the scatterer,
- σ_{bi} = biRCS,
- A_{eff} = $\lambda^2/(4\pi)$ is effective aperture area of an isotropic antenna.

In Eq. (1), there are three factors on the right side. The first factor is the power density impinging on the scatterer. The second factor is regarded as the scattering process, during which the incident power is partially intercepted and reradiated by the scatterer. Then, the scattered signal propagates toward the RX with an attenuation computed by R_r. The third factor is related to the receiving capability of the RX. Eq. (1) has the advantage of abstracting the complex scattering mechanism by using a single coefficient, biRCS, and it can be easily implemented with channel simulators [34].

In Eq. (1), the biRCS is the most important coefficient as it fully determines the feature of vehicle scattering. By using biRCS, the scatterer's capability of EM wave interception and reradiation can be quantified [33]. However, the biRCS in this study is not as simple as its original definition in far-field condition. According to far-/near-field conditions [35], the biRCS should be classified as far-field biRCS (FF-biRCS) and near-field biRCS (NF-biRCS). The former is simple, being just a function of the incident/scattered wave directions and frequency (f). The latter is more complicated as it varies with the distances ($R_{t/r}$).

The computation of vehicle scattering in channels is much easier in the far-field, since the FF-biRCS can even be obtained by a look-up table. However, FF-biRCS is inapplicable in most cases as the far-field condition is hardly satisfied. The widely accepted criterion that approximately classifies the field as being either far or near is [35]:

$$\min\{R_t, R_r\} > \frac{2 \cdot D_{\max}^2}{\lambda} \tag{2}$$

where $D_{\max}$ is the maximum dimension of the scatterer and λ is wavelength. According to Eq. (2), the FF-biRCS of a car is useful for Eq. (1) only when $R_{t/r}$ is no less than 983 m at 5.9 GHz ($D_{\max} = 5$ m); and 8850 m for a truck in the same condition ($D_{\max} = 15$ m). This far-field boundary is much further than any practical situation that has important vehicle scattering in a few dozen meters. Therefore, the modeling of vehicle scattering in V2X channels requires the modeling of its NF-biRCS.

B. NF-BIRCS CALCULATION BY USING SCs

It is known that the SCs can precisely reconstruct the near-field mono-static RCS (NF-monoRCS) [30]. In this paper, the NF-monoRCS reconstruction model in [30] is carefully extended to efficiently model NF-biRCS. Furthermore, the SCs are extracted from the far-field scattered field (E_F^s) obtained from general techniques (e.g., measurement, GO, PO), which will be explained in the next section.

To begin, the symbol E^s is used to represent the phrase "scattered field", thus $E_{F/N}^s$ indicates the E^s in specific "far-/near-field" conditions. In SCs modeling, each point is assigned with an independent strength and position $\{A, \vec{r}\}$ as representing a wave interaction at a local portion of the target. Based on the SCs, the bi-static E_N^s is calculated by vectorially summing the contributions from all valid SCs (see Fig. 3):

$$\begin{aligned} &E_N^s\left(\vec{R}_{t/r}, f\right) \\ &= \sum_i A_i \cdot \exp\left(-j\frac{2\pi f}{c}\left|\vec{r}_i - \vec{R}_t\right|\right) \cdot \left(\frac{\left|\vec{R}_t\right|}{\left|\vec{r}_i - \vec{R}_t\right|}\right) \\ &\quad \cdot \exp\left(-j\frac{2\pi f}{c}\left|\vec{R}_r - \vec{r}_i\right|\right) \cdot \left(\frac{\left|\vec{R}_r\right|}{\left|\vec{R}_r - \vec{r}_i\right|}\right) \end{aligned} \tag{3}$$

where c is the speed of light, and $\vec{R}_{t/r}$ is distance vector from the centroid of the scatterer to the TX/RX. It should

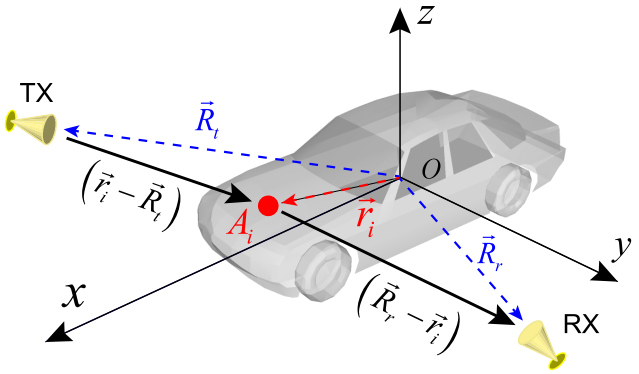

FIGURE 3. Bi-static E_N^s estimation based on SCs.

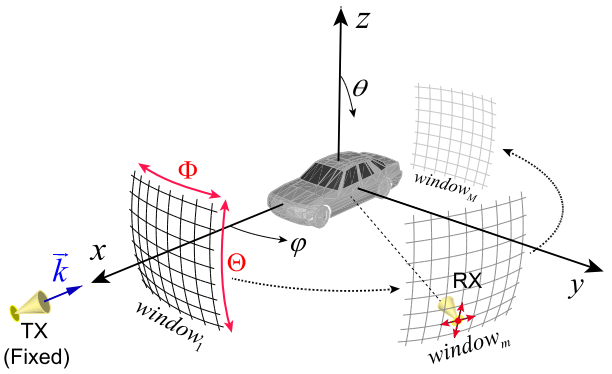

FIGURE 4. An example of collecting E_F^s for extracting SCs of vehicles.

be clarified that, since an SC is extracted from a certain frequency and aspects window (see Section III), the SC is valid for Eq. (3) only if the calculating frequency and aspects are within its extracting window.

Eq. (3) indicates that the different phase terms associated with the SCs cause the variability of E_N^s. The normalization of E_N^s and the range correction used in [30] are adopted in Eq. (3). E_N^s will be evolved into E_F^s when $\left|\vec{R}_{t/r}\right|$ approaches the far-field boundary, thus all SCs are approximately in phase [36]. Additionally, if the TX and RX are equipped with non-isotropic antennas, the $G_{t/r}$ in Eq. (1) should be accounted for earlier in Eq. (3). It is worth mentioning that Eq. (3) is derived based on the SCs obtained from single-bounce scattering mechanisms. However, the SCs obtained from multi-bounce scattering mechanisms will cause inaccuracy of this model (refer to [30]).

Next, since E_N^s has been normalized, the NF-biRCS can be directly obtained by a simple relation of [31]:

$$\sigma_{bi} = 4\pi \cdot \left|E_N^s\right|^2 \tag{4}$$

where $\left|E_N^s\right|^2$ is equal to the ratio of scattered power per unit solid angle (steradian) along the vector $\vec{R}_r$ to the power density intercepted by the scatterer.

III. EXTRACTING SCs FROM E_F^s

As discussed above, the SCs are useful to model both E_N^s and E_F^s of an electrically large scatterer. The SCs, in turn, can be obtained by processing E_F^s through inverse synthetic aperture radar (ISAR) imaging [37], a powerful signal processing technique that can display the dominant SCs on an image. In the same system configuration, the ISAR image, E_F^s and SCs are equivalent as they can be converted between each other. For brevity, the details of SCs, E_F^s and ISAR can be found in [31] and [37]–[39].

Let us explain how SCs are obtained from the initial measured/simulated E_F^s by an example. Fig. 4 provides the example of collecting the initial E_F^s, where the TX and RX are both in the far-field of the car. The angles φ and θ describe the azimuth angle and elevation angle of the incident/scattered wave (defined as $\varphi_{in/s}$ and $\theta_{in/s}$). In the example, the centroid of the car is set to be the origin of the coordinate system. The TX is fixed and always points at the origin along the direction of the negative x axis. Thus the emitted EM wave can be expressed by wave number vector $\vec{k}_{in} = k \cdot \hat{k}_{in}$ where $k = 2\pi f/c$ and $\hat{k}_{in}$ is incident unit vector defined by $\varphi_{in} = \pi$ and $\theta_{in} = \pi/2$. The $window_1$ illustrated in Fig. 4 exemplifies a collecting window of E_F^s, where the RX collects initial E_F^s at evenly spaced aspects (see the intersections) and at discrete frequencies (or k). The manner of collecting E_F^s is similar to the manner of an over-the-air (OTA) test in an anechoic chamber [40]–[42]. Correspondingly, $\vec{k}_s = k \cdot \hat{k}_s$ is defined for the scattered EM wave.

Still referring to Fig. 4, now assuming there are total N SCs overlaid on the car, and these SCs were obtained by processing the initial $E_F^s\left(k, \varphi_{in/s}, \theta_{in/s}\right)$ which was collected in $window_1$ and at a set of discrete frequencies (or k). Then, the $E_F^s\left(k, \varphi_{in/s}, \theta_{in/s}\right)$ can be approximatively reconstructed by (extended from [31]):

$$E_F^s\left(k, \varphi_{in/s}, \theta_{in/s}\right) \cong \sum_{i=1}^{N} A_i \cdot e^{-j\cdot\left(\vec{k}_s - \vec{k}_{in}\right)\cdot\vec{r}_i} \tag{5}$$

where $\vec{r}_i$ is depicted by the position (x_i, y_i, z_i) of the i-th SC, and $\vec{k}_{in}$ and $\vec{k}_s$ are calculated, respectively, as follows:

$$\begin{aligned}\vec{k}_{in} &= k \cdot \hat{k}_{in} \\ &= k \cdot \left(\hat{x} \cdot \sin\theta_{in}\cos\varphi_{in} + \hat{y} \cdot \sin\theta_{in}\sin\varphi_{in} + \hat{z} \cdot \cos\theta_{in}\right) \\ &= -k \cdot \hat{x}\end{aligned} \tag{6}$$

$$\begin{aligned}\vec{k}_s &= k \cdot \left(\hat{x} \cdot \sin\theta_s\cos\varphi_s + \hat{y} \cdot \sin\theta_s\sin\varphi_s + \hat{z} \cdot \cos\theta_s\right) \\ &= k \cdot \left(\hat{x} \cdot \cos\Delta\theta\cos\Delta\varphi + \hat{y} \cdot \cos\Delta\theta\sin\Delta\varphi + \hat{z} \cdot \sin\Delta\theta\right)\end{aligned} \tag{7}$$

where $\hat{x}, \hat{y}, \hat{z}$ are unit vectors describing x, y, z axes, and $\Delta\varphi = (\varphi_s - (\varphi_{in} + \pi))$ and $\Delta\theta = ((\pi - \theta_{in}) - \theta_s)$.

Therefore, the phase term of $\left(\vec{k}_s - \vec{k}_{in}\right) \cdot \vec{r}_i$ is rewritten as:

$$\begin{aligned}\left(\vec{k}_s - \vec{k}_{in}\right) \cdot \vec{r}_i = {} & k \cdot (1 + \cos\Delta\theta\cos\Delta\varphi) \cdot x_i \\ & + k \cdot \cos\Delta\theta\sin\Delta\varphi \cdot y_i + k \cdot \sin\Delta\theta \cdot z_i\end{aligned} \tag{8}$$

It is further assumed that the frequency bandwidth B (or wave number bandwidth B_k) of the collection is small

compared to the center frequency f_c (or center wave number k_c). The angular bandwidths Φ and Θ of $window_1$ illustrated in Fig. 4 are also assumed to be small. Thus, in this example, the following assumptions can be further obtained:

$$\begin{aligned} k &\cong k_c \\ \cos\Delta\theta\cos\Delta\varphi &\cong 1 \\ \cos\Delta\theta\sin\Delta\varphi &\cong \Delta\varphi \\ \sin\Delta\theta &\cong \Delta\theta \end{aligned} \tag{9}$$

By using Eq. (8) and Eq. (9), it follows that Eq. (5) can be reorganized as:

$$\begin{aligned} &E_F^s\left(k, \varphi_{in/s}, \theta_{in/s}\right) \\ &\quad = E_F^s\left(k, \Delta\varphi, \Delta\theta\right) \\ &\quad \cong \sum_{i=1}^{N} A_i \cdot e^{-2jkx_i} \cdot e^{-j\Delta\varphi\cdot k_c y_i} \cdot e^{-j\Delta\theta\cdot k_c z_i} \end{aligned} \tag{10}$$

Next, the three-dimensional (3D) ISAR image for the example is obtained by taking 3D inverse Fourier transform (IFT) for $E_F^s\left(k, \Delta\varphi, \Delta\theta\right)$ with respect to k, $\Delta\phi$ and $\Delta\theta$, respectively. The detailed transformation processes are derived in Eq. (11), as shown at the bottom of the next page, where $PSF\left(x, y, z\right)$ is called the point spread function (PSF) [31]. As can be seen in Eq. (11), the PSF is a function of B_k, Φ and Θ, thus, it is entirely determined by the E_F^s collecting window. Therefore, it can be concluded that the ISAR image is exactly the image which displays a set of PSF-defocused SCs.

After SCs have been successfully displayed in the ISAR image, the well-known CLEAN algorithm was selected for extracting the SCs from the image [37], [39]. The CLEAN algorithm has been widely verified as being able to extract important SCs from an ISAR image by a simple but robust iterative procedure. In the CLEAN algorithm, for each iteration, the highest SC in the image will be extracted and saved with its strength and location ($\{A, \vec{r}\}$), the relevant PSF around the SC is removed from the image and, afterward, the residual image is ready for next iteration. It is worth emphasizing that the SCs extracted from a E_F^s collecting window and within a frequency range are only able to reconstruct the E_F^s in the same angular and frequency ranges.

Notice that, although all derivations in this section are based on a specific example of collecting E_F^s as illustrated in Fig. 4, the methodology is extendible to more general situations. For example, if E_F^s is collected in $window_m$ (see Fig. 4), the relative SCs can be directly obtained when treating the E_F^s as being collected in $window_1$. Then, these relative SCs will be rotated back to their correct positions according to angular difference between $window_m$ and $window_1$. Furthermore, as shown in Fig. 4, for the purpose of being able to reconstruct car scattering of any potential direction around horizontal plane, the E_F^s from a total of M continuous windows are collected and all SCs are extracted. In next section, the accuracy of proposed methodology of extracting SCs will be validated.

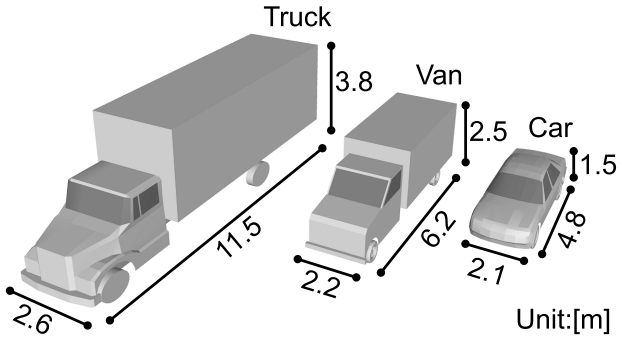

FIGURE 5. The geometries of three standard vehicles and their 3D dimensions.

IV. PERFORMANCE EVALUATION OF THE PROPOSED MODEL

As mentioned previously, this paper seeks to establish a technically sound methodology for calculating the scattered power of vehicles with good accuracy and low computation time. The SCs extracted from well-collected E_F^s can analytically reconstruct E_N^s and NF-biRCS. In this section, the accuracy of SCs extraction procedure is first validated on three standard vehicles (see Fig. 5). Then, based on these SCs, the near-field scattering power of vehicles is reconstructed and compared to the results from PO. Although, it will be demonstrated that the proposed model is fairly accurate and very efficient, the accuracy of the model decreases obviously at very close-in ranges.

The digital geometries of three investigated vehicles are shown in Fig. 5. The advantage of adopting such vehicles is that the significant geometric differences allow the validation to be more comprehensive. Furthermore, the geometries are actually quite simple in this study as some vehicle structural details like side mirrors, handlebars, windshield wipers, wheels, etc. were omitted or simplified, and all geometries were assumed to be made of a perfect conductor. The main reason is that in the stage of massively PO simulation, too many details will significantly increase the overall computational time, but the improvement from considering such details is quite small in the validation of the proposed model.

A. THE 3D SCS EXTRACTED FROM E_F^s

Fig. 6 illustrates a configuration for directly collecting E_F^s data after embedding the digital geometry into full-wave analysis software which, in this study, is commercial *FEKO* 7.0 [43]. The *FEKO* has been verified as being qualified for calculating the E_F^s of electrically large structures in many publications [44], [45]. The configuration includes the frequency range, angular window/interval and full-wave method (PO) selected for the E_F^s collection. Similar to Fig. 4, the collecting configuration displayed in the Fig. 6 exemplifies the overall requested data grid of E_F^s around the horizontal plane (when the incident wave arrives with $\varphi_{in} = \pi$ and $\theta_{in} = \pi/2$). Due to the symmetry of the car, in this example,

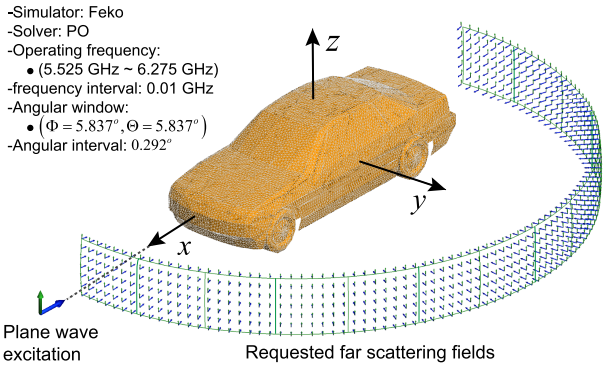

FIGURE 6. Collecting E_F^s from *FEKO* software where green arrow indicates the vertical polarization and blue arrow indicates the direction.

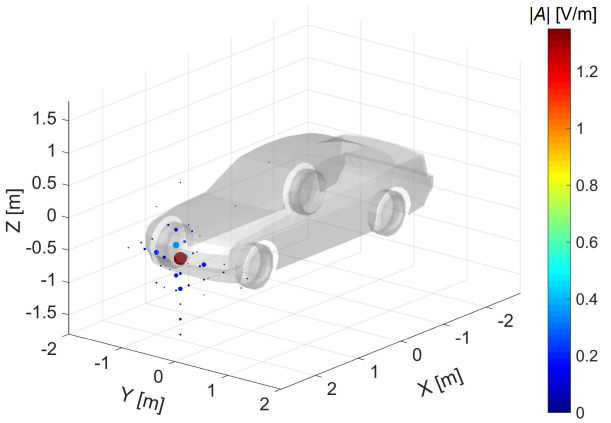

FIGURE 7. Geometry of the car and the extracted SCs from *window*$_1$.

TABLE 1. ME, Std and RMSE between PO-simulated and SCs-reconstructed FF-biRCS.

[dB]	ME	Std	RMSE
Car	0.01	0.52	0.52
Van	0.01	1.58	1.58
Truck	0.01	2.42	2.43

the E_F^s data in the first two quadrants is only requested. Then, the collected E_F^s data is partitioned into continuous windows for ISAR imaging and SCs extraction as described in section III. In the study, although 100 SCs were extracted from each window, only a few SCs (called dominant SCs) have a strong amplitude that is significantly higher than the others. The dominant SCs are located on/around the vehicle and they are representative of the scattering mechanisms on vehicle surface (see Fig. 2). In addition, a number of SCs that have tiny amplitudes are located beyond the vehicle's outline, these SCs are the noise in the residual ISAR image [31]. Fig. 7 plots the geometry of the car and the extracted SCs from *window*$_1$. In this example, since the car head is the main contributor as causing the E_F^s of *window*$_1$, it is evident that the dominant SCs are located at the car head.

After SCs of each window are extracted, the accuracy of all SCs should be verified. Here, as mentioned earlier, the E_F^s, ISAR, and SCs are equivalent as they can be converted between each other. Moreover, the E_F^s can be directly converted into FF-biRCS which is more straightforward (see Eq. (4)). Therefore, in this study, the SCs-reconstructed FF-biRCSs of three vehicles are compared to the PO-simulated results as a function of φ_s. Fig. 8 displays the comparison results. Observe that the FF-biRCS predicted by SCs agrees consistently with the PO simulation results in all cases. The statistical differences between the two results are listed in Table 1 according to mean error (ME), standard deviation (Std), and root mean square error (RMSE). Observe that, for any vehicle, the ME is only 0.01 dB and also the Std/RMSE is no greater than 2.43 dB, which indicates that the technique of SCs extraction is fairly robust. However, when the vehicle becomes bigger (from car to truck), some minor imperfections are observed as Std/RMSE increases by around 2 dB. The main reason is that, according to Eq. (5), the reconstructed E_F^s is obtained by vertically summing up contributions of all available SCs. This summation causes spatial fluctuation of E_F^s due to constructive/destructive interference. Once vehicles become bigger, the number of dominant SCs increases accordingly, thus making the spatial fluctuations more severe. So, the lines of the truck in Fig. 8 are much rougher. More important, since the vehicle becomes bigger, any slight displacement of SCs will cause a larger imperfection of reconstruction results as shown in Table 1. This phenomenon will be significant in predicting near-field scattering, which will be detailed later.

$$
\begin{aligned}
ISAR\left(x,y,z\right) &\triangleq \mathscr{F}_3^{-1}\left\{E_F^s\left(k,\Delta\varphi,\Delta\theta\right)\right\} = \mathscr{F}_3^{-1}\left\{\sum\nolimits_{i=1}^{N} A_i\cdot e^{-2jkx_i}\cdot e^{-j\Delta\varphi\cdot k_c y_i}\cdot e^{-j\Delta\theta\cdot k_c z_i}\right\} \\
&= \sum\nolimits_{i=1}^{N} A_i\cdot \int_{k_c-\frac{B_k}{2}}^{k_c+\frac{B_k}{2}} e^{j2\pi\left(\frac{k}{\pi}\right)\cdot(x-x_i)} d\left(\frac{k}{\pi}\right)\cdot \int_{-\frac{\Phi}{2}}^{\frac{\Phi}{2}} e^{j2\pi\left(\frac{\Delta\varphi\cdot k_c}{2\pi}\right)\cdot(y-y_i)} d\left(\frac{\Delta\varphi\cdot k_c}{2\pi}\right)\cdot \int_{\frac{-\Theta}{2}}^{\frac{\Theta}{2}} e^{j2\pi\left(\frac{\Delta\theta\cdot k_c}{2\pi}\right)\cdot(z-z_i)} d\left(\frac{\Delta\theta\cdot k_c}{2\pi}\right) \\
&= \sum\nolimits_{i=1}^{N} A_i\cdot e^{j2k_c\cdot(x-x_i)}\cdot \frac{\sin\left(B_k\left(x-x_i\right)\right)}{\pi\left(x-x_i\right)}\cdot \frac{\sin\left(\frac{\Phi}{2}k_c\left(y-y_i\right)\right)}{\pi\left(y-y_i\right)}\cdot \frac{\sin\left(\frac{\Theta}{2}k_c\left(z-z_i\right)\right)}{\pi\left(z-z_i\right)} \\
&= \sum\nolimits_{i=1}^{N} A_i\cdot PSF\left(x-x_i,y-y_i,z-z_i\right)
\end{aligned}
\tag{11}
$$

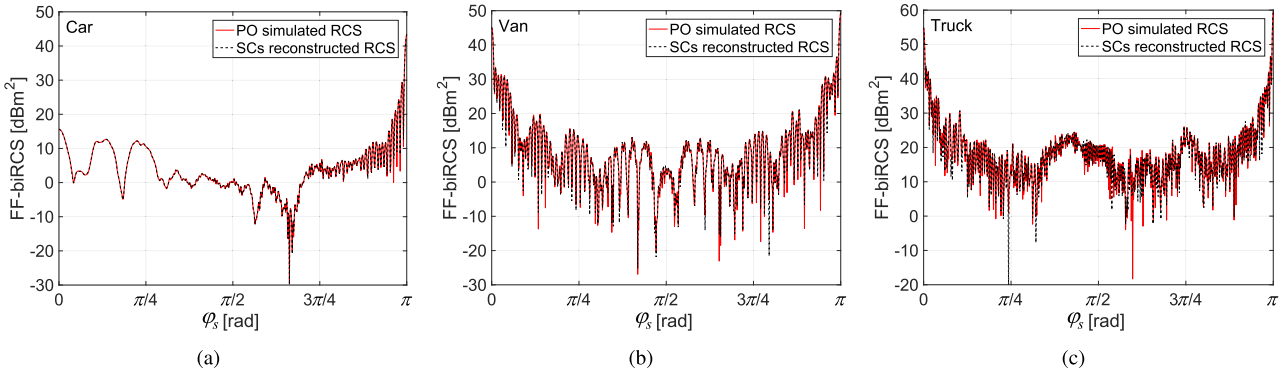

FIGURE 8. Comparisons of the FF-biRCS computed by SCs and PO for the three vehicles at 5.9 GHz. (a) car; (b) van; (c) truck.

B. PERFORMANCE OF RECONSTRUCTING NEAR-FIELD SCATTERING

Based on the verified SCs, the performance of proposed model described in Section II is now demonstrated. In the near-field, for any vehicle, the SCs-reconstructed scattering power is compared to the PO simulated result as a function of the TX/RX range. The TX was set as a vertically polarized electric current dipole (formed by two conductors with a total length dl), the magnitude of the dipole was set as $Idl = 1\,A{\cdot}m$ where I is the current over the dipole; the RX was assumed to be an isotropic and vertically polarized antenna with 0 dBi antenna gain. Since the SCs were extracted at scattered directions around the horizontal plane, the scattering power is only computed in the horizontal plane (refer to section IV-A).

In the evaluation, the centroid of the vehicle is set at the origin of the coordinate axis. Once the TX is fixed with a distance of R_t to the origin, the scattering power of the vehicle will be computed in a horizontal annulus centered at the origin (i.e., computation is in the range of $R_t \le R_r \le R_t + R_D$, $0 \le \varphi_s \le 2\pi$ and $\theta_s = \pi/2$, where R_D is defined as the annular width). For example, Fig. 9 gives results computed by PO and SCs at 5.9 GHz when the TX is fixed in front of the car, where $R_t = 20$ m and $R_D = 30$ m. On the whole, the agreement between the two results is very good. Although the SCs model underestimates the scattered power at some RX positions, the SCs-reconstructed scattered power still follows a similar scattered power pattern as computed by PO. For the numerical difference between Fig. 9(a) and Fig. 9(b), the ME is as low as -0.91 dB and Std/RMSE are both around 1.80 dB. Additionally, the computation time of SCs and PO in Fig. 9 is important. Since the same laptop was used (12 GB RAM and total 8 CPUs each with 2.7 GHz frequency), the time for PO is 108 s while it is only 6 s for SCs, which indicates the proposed model is more useful for extensive simulations.

In this study, the performance of the proposed model is evaluated in a reasonable range of TX. More specifically, the statistical values of the numerical difference shown in Fig. 9 are repeatedly computed at different R_t while $R_D = 20$ m. According to the dimensions of three vehicles,

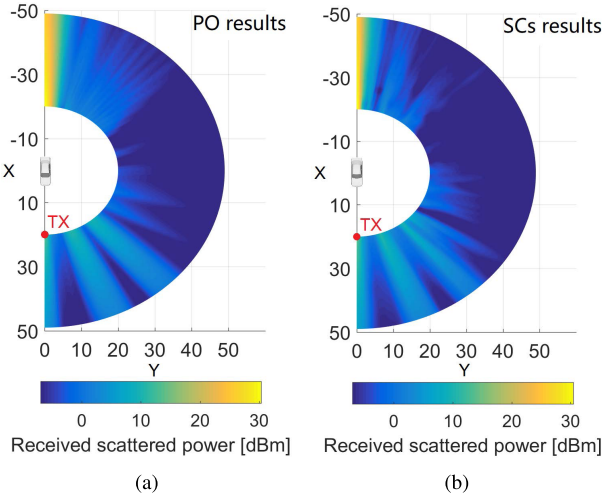

FIGURE 9. An example of the comparison of the near-field scattered power computed by SCs and PO for the car, where $R_t = 20$ m, $R_D = 30$ m. (a) PO results; (b) SCs results.

the ranges of R_t for the car, the van, and the truck are $5 \sim 100$ m, $10 \sim 100$ m and $10 \sim 100$ m, respectively. The maximum range was selected from an assumption that the application scenarios of the proposed model are mostly less than 100 m. Furthermore, some publications (e.g. [46], [47]) directly use FF-biRCS for near-field calculation. To benchmark the improvement of the proposed model, the scattering power as calculated by FF-biRCS is used as a reference.

Fig. 10 shows the statistical values of differences as the function of R_t. It is apparent that all values decrease significantly as the lines converge rapidly before $R_t < 50$ m. Most important, the performance of proposed models is undoubtedly better than directly using FF-biRCS. However, for R_t in the range $50 \sim 100$ m, using FF-biRCS directly is quite profitable for the car(van) case, which indicates that the far-field criterion of Eq. (2) is moderate, since the theoretical value for directly using FF-biRCS of car(van) should be 983 m(2273 m). Since the truck is much bigger, an acceptable result of directly using FF-biRCS is only obtained after 100 m. Furthermore, comparing the results among three

TABLE 2. The values of R_t captured at some key thresholds of the statistics in Fig. 10.

	SCs vs. PO (red lines in Fig. 10)									FF-biRCS vs. PO (black dotted lines in Fig. 10)								
R_t at key	ME [dB]			Std [dB]			RMSE [dB]			ME [dB]			Std [dB]			RMSE [dB]		
thresholds	=5	=3	=1	=5	=3	=1	=5	=3	=1	=5	=3	=1	=5	=3	=1	=5	=3	=1
Car [m]	<5	<5	16.8	<5	8.6	43.1	<5	10.1	50.2	<5	7.3	23.8	<5	10.6	80.0	6.9	13.8	83.7
Van [m]	10.0	21.1	76.9	13.3	21.2	>100	22.3	43.2	>100	20.8	34.3	≈100	21.2	52.9	>100	40.4	69.4	>100
Truck [m]	18.7	35.9	≈100	16.3	30.2	>100	25.9	45.0	>100	50.0	92.8	>100	48.3	>100	>100	≈100	>100	>100

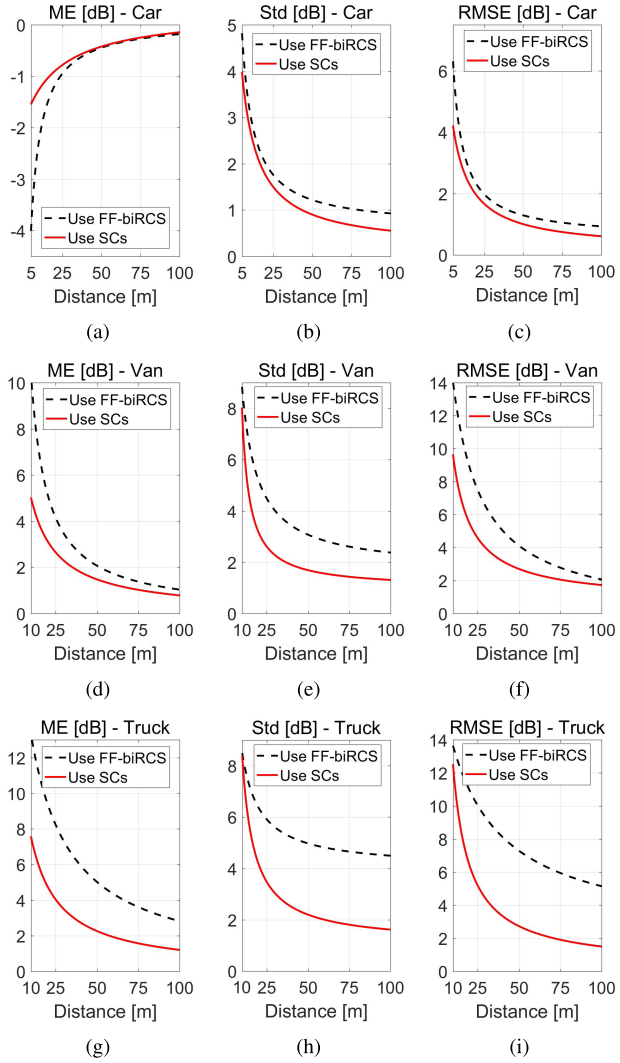

FIGURE 10. Statistical values of differences as a function of R_t, where the red lines indicate the difference between SCs-reconstructed results and PO-simulated results; the black dotted lines indicate the difference between results calculated directly from FF-biRCS and PO-simulated results. (a), (b) and (c) are the ME, Std, RMSE in the car case; (d), (e) and (f) are the ME, Std, RMSE in the van case; (g), (h) and (i) are the ME, Std, RMSE in the truck case.

vehicles, the gap between the red and black dotted lines increases according to the increasing size of vehicles. This phenomenon indicates the consistency of proposed model is better than that of directly using FF-biRCS, since the former is less sensitive to the size of vehicles.

To further elaborate on the statistics shown in Fig. 10, the values of R_t captured at some key thresholds of the statistics are listed in Table 2. To be more concise, the phrase "red lines"/"black dotted lines" is directly used to represent the more rigorous description of "statistical values of the difference between SCs-reconstructed results and PO-simulated results"/"statistical values of the difference between FF-biRCS-computed results and PO-simulated results". From Table 2, notice that, for the car, all three statistics of red lines will be lower than 1 dB as long as the R_t is larger than 50.2 m. However, still, for the car, the R_t for black dotted lines should be larger than 83.7 m to meet the same performance. The van/truck shows worse performance since almost all statistics are larger than 1 dB in the first 100 m. The maximum numerical gap between red and black dotted lines can be observed for case of the truck, i.e., taking 5 dB as a threshold, all R_t of black dotted lines are approximately triple that of red lines. Moreover, in Table 2, the minimum numerical gap among vehicles can be found in red lines between van and truck, e.g., the R_t regarding Std=5 dB increases from 13.3 m to 16.3 m, and R_t regarding RMSE=3 dB increases by only 1.8 m. However, for black dotted lines, by contrast, the gaps between van and truck are strikingly large in the same situation.

In conclusion, the performance of the proposed model is always better than that of directly using FF-biRCS; especially for car scattering, the model gives an excellent performance for R_t in the range of a few dozen meters. Nevertheless, the model is not always reliable in the very close-in range, because, according to the explanation discussed in [30], the SCs themselves will be defocused in the very close-in range, which may make the SCs assumption no longer valid. Besides, as expected, the proposed model is still less than ideal for larger vehicles, which could be attributed to the reason discussed in Section IV-A that larger vehicles increase the number of dominant SCs and unavoidably increase the spatial fluctuation of predicted scattering. Despite these imperfections, after considering the efficiency of the proposed model in providing a good accuracy in a very short period, the model is practically useful for predicting vehicle scattering in V2X channel simulations.

V. CONCLUSION

This paper presented an analytical model to predict the near-field bi-static scattering of vehicles by taking advantage of the SCs of vehicles. As the accuracy of extracted SCs is directly related to the proposed model, a general methodology was subsequently derived for properly extracting SCs from E_F^s. In the methodology, there is no limit to the means of generating E_F^s. Also, the derivation of the methodology may lead

to an understanding of the cause-and-effect relationship of the scattering phenomena from vehicles. In our performance evaluations, three standard vehicles (car, van, and truck) were employed and studied at the center frequency of 5.9 GHz. Since the scattering of vehicles in V2X commonly takes place around the horizontal plane, the final validations of the proposed model were conducted in the horizontal plane. The results validate that the SCs can be extracted with high accuracy. Most important, based on these SCs, the proposed model can predict near-field bi-static scattering of vehicles with good accuracy and computational efficiency, however, its accuracy mildly degrades with the increasing size of vehicles.

To the knowledge of the authors, as being the critical improvement of [29] and [30], this study is significantly different from traditional deterministic/stochastic models because it successfully considers the balance between computational efficiency and accuracy. Additionally, it is worth mentioning that our SCs-based model has great flexibility. Once the SCs of a certain vehicle are obtained, these SCs and the vehicle can be infinitely adopted in different V2X scenarios and antenna configurations. Future work may combine this model with a traffic mobility model to obtain more complex but realistic V2X channel models. Finally, our model could be applied to a wide range of V2X channel simulations and may become an important driving force for the development of V2X applications.

REFERENCES

[1] H. Hartenstein and L. P. Laberteaux, "A tutorial survey on vehicular ad hoc networks," *IEEE Commun. Mag.*, vol. 46, no. 6, pp. 164–171, Jun. 2008.

[2] Y. He, D. Sun, M. Zhao, and S. Cheng, "Cooperative driving and lane changing modeling for connected vehicles in the vicinity of traffic signals: A cyber-physical perspective," *IEEE Access*, vol. 6, p. 13891–13897, 2018.

[3] J. Gozálvez, M. Sepulcre, and R. Bauza, "IEEE 802.11p vehicle to infrastructure communications in urban environments," *IEEE Commun. Mag.*, vol. 50, no. 5, pp. 176–183, May 2012.

[4] P. Papadimitratos, A. De La Fortelle, K. Evenssen, R. Brignolo, and S. Cosenza, "Vehicular communication systems: Enabling technologies, applications, and future outlook on intelligent transportation," *IEEE Commun. Mag.*, vol. 47, no. 11, pp. 84–95, Nov. 2009.

[5] H. Jiang, Z. Zhang, J. Dang, and L. Wu, "A novel 3-D massive MIMO channel model for vehicle-to-vehicle communication environments," *IEEE Trans. Commun.*, vol. 66, no. 1, pp. 79–90, Jan. 2018.

[6] W. Fan, T. Jämsä, J. Ø. Nielsen, and G. F. Pedersen, "On angular sampling methods for 3-D spatial channel models," *IEEE Antennas Wireless Propag. Lett.*, vol. 14, pp. 531–534, 2015.

[7] B. Ai *et al.*, "On indoor millimeter wave massive MIMO channels: Measurement and simulation," *IEEE J. Sel. Areas Commun.*, vol. 35, no. 7, pp. 1678–1690, Jul. 2017.

[8] X. Zhao, S. Li, Q. Wang, M. Wang, S. Sun, and W. Hong, "Channel measurements, modeling, simulation and validation at 32 GHz in outdoor microcells for 5G radio systems," *IEEE Access*, vol. 5, pp. 1062–1072, 2017.

[9] B. Ai *et al.*, "Challenges toward wireless communications for high-speed railway," *IEEE Trans. Intell. Transp. Syst.*, vol. 15, no. 5, pp. 2143–2158, Oct. 2014.

[10] B. Ai *et al.*, "Future railway services-oriented mobile communications network," *IEEE Commun. Mag.*, vol. 53, no. 10, pp. 78–85, Oct. 2015.

[11] D. W. Matolak, "V2V communication channels: State of knowledge, new results, and what's next," in *Proc. Int. Workshop Commun. Technol. Vehicles*. Berlin, Germany: Springer, 2013, pp. 1–21.

[12] X. Cheng, Q. Yao, M. Wen, C.-X. Wang, L.-Y. Song, and B.-L. Jiao, "Wideband channel modeling and intercarrier interference cancellation for vehicle-to-vehicle communication systems," *IEEE J. Sel. Areas Commun.*, vol. 31, no. 9, pp. 434–448, Sep. 2013.

[13] X. Zhao, X. Liang, S. Li, and B. Ai, "Two-cylinder and multi-ring GBSSM for realizing and modeling of vehicle-to-vehicle wideband MIMO channels," *IEEE Trans. Intell. Transp. Syst.*, vol. 17, no. 10, pp. 2787–2799, Oct. 2016.

[14] R. He, A. F. Molisch, F. Tufvesson, Z. Zhong, B. Ai, and T. Zhang, "Vehicle-to-vehicle channel models with large vehicle obstructions," in *Proc. IEEE Int. Conf. Commun. (ICC)*, Jun. 2014, pp. 5647–5652.

[15] R. He, A. F. Molisch, F. Tufvesson, Z. Zhong, B. Ai, and T. Zhang, "Vehicle-to-vehicle propagation models with large vehicle obstructions," *IEEE Trans. Intell. Transp. Syst.*, vol. 15, no. 5, pp. 2237–2248, Oct. 2014.

[16] Q. Wang, D. W. Matolak, and B. Ai, "Shadowing characterization for 5-GHz vehicle-to-vehicle channels," *IEEE Trans. Veh. Technol.*, vol. 67, no. 3, pp. 1855–1866, Mar. 2018.

[17] T. Abbas, K. Sjöberg, J. Karedal, and F. Tufvesson, "A measurement based shadow fading model for vehicle-to-vehicle network simulations," *Int. J. Antennas Propag.*, vol. 2015, pp. 1–12, May 2015.

[18] R. Meireles, M. Boban, P. Steenkiste, O. Tonguz, and J. Barros, "Experimental study on the impact of vehicular obstructions in VANETs," in *Proc. IEEE Veh. Netw. Conf.*, Dec. 2010, pp. 338–345.

[19] L. Cheng, B. E. Henty, D. D. Stancil, F. Bai, and P. Mudalige, "Mobile vehicle-to-vehicle narrow-band channel measurement and characterization of the 5.9 GHz dedicated short range communication (DSRC) frequency band," *IEEE J. Sel. Areas Commun.*, vol. 25, no. 8, pp. 1501–1516, Oct. 2007.

[20] A. Paier *et al.*, "First results from car-to-car and car-to-infrastructure radio channel measurements at 5.2 GHZ," in *Proc. IEEE 18th Int. Symp. Pers., Indoor Mobile Radio Commun.*, Sep. 2007, pp. 1–5.

[21] A. Paier *et al.*, "Car-to-car radio channel measurements at 5 GHz: Pathloss, power-delay profile, and delay-Doppler spectrum," in *Proc. 4th Int. Symp. Wireless Commun. Syst.*, Oct. 2007, pp. 224–228.

[22] L. Cheng, B. E. Henty, R. Cooper, D. D. Stancil, and F. Bai, "A measurement study of time-scaled 802.11a waveforms over the mobile-to-mobile vehicular channel at 5.9 GHz," *IEEE Commun. Mag.*, vol. 46, no. 5, pp. 84–91, May 2008.

[23] J. Karedal *et al.*, "A geometry-based stochastic MIMO model for vehicle-to-vehicle communications," *IEEE Trans. Wireless Commun.*, vol. 8, no. 7, pp. 3646–3657, Jul. 2009.

[24] L. Bernadó, T. Zemen, F. Tufvesson, A. F. Molisch, and C. F. Mecklenbräuker, "Delay and Doppler spreads of nonstationary vehicular channels for safety-relevant scenarios," *IEEE Trans. Veh. Technol.*, vol. 63, no. 1, pp. 82–93, Jan. 2014.

[25] I. Rodriguez *et al.*, "Measurement-based evaluation of the impact of large vehicle shadowing on V2X communications," in *Proc. 22th Eur. Wireless Conf.*, May 2016, pp. 1–8.

[26] Z. Yun and M. F. Iskander, "Ray tracing for radio propagation modeling: Principles and applications," *IEEE Access*, vol. 3, pp. 1089–1100, 2015.

[27] M. Boban, T. T. V. Vinhoza, M. Ferreira, J. Barros, and O. K. Tonguz, "Impact of vehicles as obstacles in vehicular ad hoc networks," *IEEE J. Sel. Areas Commun.*, vol. 29, no. 1, pp. 15–28, Jan. 2011.

[28] D. Vlastaras, R. Whiton, and F. Tufvesson, "A model for power contributions from diffraction around a truck in vehicle-to-vehicle communications," in *Proc. 15th Int. Conf. ITS Telecommun. (ITST)*, May 2017, pp. 1–6.

[29] H. Buddendick and T. F. Eibert, "Incoherent scattering-center representations and parameterizations for automobiles [EM programmer's notebook]," *IEEE Antennas Propag. Mag.*, vol. 54, no. 1, pp. 140–148, Feb. 2012.

[30] R. Bhalla and H. Ling, "Near-field signature prediction using far-field scattering centers extracted from the shooting and bouncing ray technique," *IEEE Trans. Antennas Propag.*, vol. 48, no. 2, pp. 337–338, Feb. 2000.

[31] C. Özdemir, *Inverse Synthetic Aperture Radar Imaging With MATLAB Algorithms*, vol. 210. Hoboken, NJ, USA: Wiley, 2012.

[32] R. S. Longhurst, *Geometrical and Physical Optics*. India, Hyderabad: Orient BlackSwan, 1970.

[33] M. I. Skolnik, *Radar Handbook* (Electronics Electrical Engineering), 3rd ed. New York, NY, USA: McGraw-Hill, 2008. [Online]. Available: https://books.google.com/books?id=76uF2Xebm-gC

[34] K. Guan *et al.*, "On the influence of scattering from traffic signs in vehicle-to-X communications," *IEEE Trans. Veh. Technol.*, vol. 65, no. 8, pp. 5835–5849, Aug. 2016.

[35] V. Degli-Esposti, F. Fuschini, E. M. Vitucci, and G. Falciasecca, "Speed-up techniques for ray tracing field prediction models," *IEEE Trans. Antennas Propag.*, vol. 57, no. 5, pp. 1469–1480, May 2009.
[36] J. M. Taylor and A. J. Terzuoli, "On the concept of near field radar cross section," in *IEEE Antennas Propag. Soc. Int. Symp. Dig.*, vol. 2, Jul. 1997, pp. 1172–1175.
[37] R. Bhalla and H. Ling, "Three-dimensional scattering center extraction using the shooting and bouncing ray technique," *IEEE Trans. Antennas Propag.*, vol. 44, no. 11, pp. 1445–1453, Nov. 1996.
[38] R. Bhalla, J. Moore, and H. Ling, "A global scattering center representation of complex targets using the shooting and bouncing ray technique," *IEEE Trans. Antennas Propag.*, vol. 45, no. 12, pp. 1850–1856, Dec. 1997.
[39] R. Bhalla, H. Ling, J. Moore, D. J. Andersh, S. W. Lee, and J. Hughes, "3D scattering center representation of complex targets using the shooting and bouncing ray technique: A review," *IEEE Antennas Propag. Mag.*, vol. 40, no. 5, pp. 30–39, Oct. 1998.
[40] W. Fan, I. Carton, P. Kyösti, and G. F. Pedersen, "Emulating ray-tracing channels in multiprobe anechoic chamber setups for virtual drive testing," *IEEE Trans. Antennas Propag.*, vol. 64, no. 2, pp. 730–739, Feb. 2016.
[41] W. Fan *et al.*, "A step toward 5G in 2020: Low-cost OTA performance evaluation of massive MIMO base stations," *IEEE Antennas Propag. Mag.*, vol. 59, no. 1, pp. 38–47, Feb. 2017.
[42] X. Chen, W. Fan, L. Hentilä, P. Kyösti, and G. F. Pedersen, "Throughput modeling and validations for MIMO-OTA testing with arbitrary multi-path," *IEEE Antennas Wireless Propag. Lett.*, vol. 17, no. 4, pp. 637–640, Apr. 2018.
[43] *FEKO Simulation Software*. Accessed: Dec. 23, 2018. [Online]. Available: http://www.feko.info/
[44] J. Dai and Y.-Q. Jin, "Scattering simulation and reconstruction of a 3-D complex target using downward-looking step-frequency radar," *IEEE Trans. Geosci. Remote Sens.*, vol. 49, no. 10, pp. 4035–4047, Oct. 2011.
[45] M. Chen and C.-C. Chen, "RCS patterns of pedestrians at 76∼77 GHz," *IEEE Antennas Propag. Mag.*, vol. 56, no. 4, pp. 252–263, Aug. 2014.
[46] K. I. Ziri-Castro, W. G. Scanlon, and N. E. Evans, "Prediction of variation in MIMO channel capacity for the populated indoor environment using a radar cross-section-based pedestrian model," *IEEE Trans. Wireless Commun.*, vol. 4, no. 3, pp. 1186–1194, May 2005.
[47] L. Tian, V. Degli-Esposti, E. M. Vitucci, and X. Yin, "Semi-deterministic radio channel modeling based on graph theory and ray-tracing," *IEEE Trans. Antennas Propag.*, vol. 64, no. 6, pp. 2475–2486, Jun. 2016.

GUANGKAI LI (S'15) received the B.E. degree from Anhui Jianzhu University, in 2010. He is currently pursuing the Ph.D. degree with the State Key Laboratory of Rail Traffic Control and Safety, Beijing Jiaotong University, Beijing, China. He is currently visiting the Georgia Institute of Technology, Georgia, USA, supported by the China Scholarship Council for one year. His research interests include optimizing ray tracing algorithm based on measurements, deterministic channel modeling in dynamic scenarios, and efficiently modeling important scatterers in channel simulations.

BO AI (M'00–SM'10) received the M.S. and Ph.D. degrees from Xidian University, Xi'an, China, in 2002 and 2004, respectively. He was with Tsinghua University, Beijing, China, where he was an Excellent Post-Doctoral Research Fellow, in 2007. He is currently a Professor and an Advisor of Ph.D. candidates with Beijing Jiaotong University, Beijing, where he is also the Deputy Director of the State Key Laboratory of Rail Traffic Control and Safety. He is also with the Engineering College, Armed Police Force, Xi'an. His interests include the research and applications of orthogonal frequency-division multiplexing techniques, high-power amplifier linearization techniques, radio propagation and channel modeling, global systems for mobile communications for railway systems, and long-term evolution for railway systems. He has authored or co-authored six books and 270 scientific research papers, and holds 26 invention patents in his research areas.

Dr. Ai is a Fellow of the Institution of Engineering and Technology. He is an Editorial Committee Member of the *Wireless Personal Communications Journal*. He received many awards such as the Qiushi Outstanding Youth Award by the HongKong Qiushi Foundation, the New Century Talents by the Chinese Ministry of Education, the Zhan Tianyou Railway Science and Technology Award by the Chinese Ministry of Railways, and the Science and Technology New Star by the Beijing Municipal Science and Technology Commission. He was as a Co-Chair or a Session/Track Chair of many international conferences such as the 9th International Heavy Haul Conference, in 2009, the 2011 IEEE International Conference on Intelligent Rail Transportation, HSRCom2011, the 2012 IEEE International Symposium on Consumer Electronics, the 2013 International Conference on Wireless, Mobile and Multimedia, the IEEE Green HetNet 2013, and the IEEE 78th Vehicular Technology Conference in 2014. He is an Associate Editor of the IEEE TRANSACTIONS ON CONSUMER ELECTRONICS.

GORDON L. STÜBER (S'81–M'82–SM'96–F'99) received the B.A.Sc. and Ph.D. degrees in electrical engineering from the University of Waterloo, ON, Canada, in 1982 and 1986, respectively. In 1986, he joined the School of Electrical and Computer Engineering, Georgia Institute of Technology, where he is currently the Joseph M. Pettit Chair Professor of communications.

Dr. Stüber has authored wireless textbook *Principles of Mobile Communication* (Kluwer Academic Publishers, 1996, 2001, 2011, 2017). He was a co-recipient of the Jack Neubauer Memorial Award, in 1997, for the best systems paper published in the IEEE TRANSACTIONS ON VEHICULAR TECHNOLOGY. He was a recipient of the IEEE Vehicular Technology Society James R. Evans Avant Garde Award, in 2003, for his contributions to theoretical research in wireless communications, the 2007 IEEE Communications Society Wireless Communications Technical Committee Recognition Award for outstanding technical contributions in the field and for service to the scientific and engineering communities, and the 2017 IEEE ComSoc RCC Technical Recognition Award for outstanding research contributions to radio communications. He was a co-recipient of the Neal Shepherd Memorial Best Propagation Paper Award, in 2012, for the best propagation paper published in the IEEE TRANSACTIONS ON VEHICULAR TECHNOLOGY. He was an IEEE Communication Society Distinguished Lecturer, in 2007 and 2008, and the IEEE Vehicular Technology Society Distinguished Lecturer, from 2010 to 2012.

Dr. Stüber was a member of the IEEE Communications Society Awards Committee, from 1999 to 2002. He served as an Elected Member-at-Large for the IEEE Communications Society Board of Governors, from 2007 to 2009. He has been an Elected Member of the IEEE Vehicular Technology Society Board of Governors, since 2001. He received the IEEE Vehicular Technology Society Outstanding Service Award, in 2005. He served as the Technical Program Chair for the 1996 IEEE Vehicular Technology Conference and the 1998 IEEE International Conference on Communications, and the General Chair for the Fifth IEEE Workshop on Multimedia, Multiaccess and Teletraffic for Wireless Communications, in 2000, the 2002 IEEE Communication Theory Workshop, and the Fifth YRP International Symposium on Wireless Personal Multi-media Communications, in 2002. He was an Editor of Spread Spectrum with the IEEE TRANSACTIONS ON COMMUNICATIONS, from 1993 to 1998.

KE GUAN (S'10–M'13) received the B.E. and Ph.D. degrees from Beijing Jiaotong University in 2006 and 2014, respectively. In 2009, he joined the Universidad Politécnica de Madrid, Spain, as a Visiting Scholar. From 2011 to 2013, he was a Research Scholar with the Institut für Nachrichtentechnik, Technische Universität Braunschweig, Germany. From 2013 to 2014, he was invited to conduct joint research with the Universidad Politécnica de Madrid, Spain. He is currently an Associate Professor with the State Key Laboratory of Rail Traffic Control and Safety and the School of Electronic and Information Engineering, Beijing Jiaotong University. His current research interests include the field of measurement and modeling of wireless propagation channels, high-speed railway communications, vehicle-to-x channel characterization, and indoor channel characterization for high-speed short-range systems including future terahertz communication systems. He was a recipient of the Huawei Excellent Student Award of China, in 2013, the First National Scholarship for Ph.D. candidates, in 2012, the Humboldt Research Fellowship for Post-Doctoral Researchers, in 2015, and the 2014 International Union of Radio Science Young Scientist Award. His papers received six best paper awards.

Dr. Guan has authored or co-authored two books and one book chapter, and more than 160 journal and conference papers. He holds one patent. He is a member of the IC1004 and CA15104 initiatives. He is the Pole Leader of the European Railway Research Network of Excellence. He is an Editor of the IEEE Access, the *IET Microwave, Antenna & Propagation*, and *Physical Communication*, and a Guest Editor of the IEEE Transactions on Vehicular Technology. He serves as a Publicity Chair for PIMRC 2016 and ITST 2018, a Track Co-Chair for EuCNC, the Session Convener for EuCAP, from 2015 to 2018, and a TPC Member for many IEEE conferences, such as GLOBECOM, ICC, and VTC.

GUOWEI SHI received the M.S. and Ph.D. degrees in electrical engineering from Northwestern Polytechnical University, China, in 1998 and 2001, respectively. He is currently a Senior Research Staff with the China Academy of Telecommunication Research, Beijing, China. He focused on network optimization, network architecture, mesh networking, and M2M communications. His research interests include communication theory, networking, and information theory.